ACS APPLIED MATERIALS & INTERFACES

Research Article

www.acsami.org

Reversibility and Stability of ZnO-Sb_2Te_3 Nanocomposite Films for Phase Change Memory Applications

Guoxiang Wang,*[,†] Yimin Chen,[‡] Xiang Shen,*[,†] Junjian Li,[‡] Rongping Wang,[§] Yegang Lu,[‡] Shixun Dai,[†] Tiefeng Xu,[†,‡] and Qiuhua Nie*[,†,‡]

[†]Laboratory of Infrared Material and Devices, The Advanced Technology Research Institute, Ningbo University, Ningbo 315211, Zhejiang, China

[‡]Faculty of Information Science and Engineering, Ningbo University, Ningbo 315211, Zhejiang, China

[§]Laser Physics Centre, Research School of Physics and Engineering, Australian National University, Canberra, ACT 0200, Australia

ABSTRACT: $(ZnO)_x(Sb_2Te_3)_{1-x}$ materials with different ZnO contents have been systemically studied with an aim of finding the most suitable composition for phase change memory applications. It was found that ZnO-doping could improve thermal stability and electrical behavior of Sb_2Te_3 film. Sb_2Te_3-rich nanocrystals, surrounded by ZnO-rich amorphous phases, were observed in annealed ZnO-doped Sb_2Te_3 composite films, and the segregated domains exhibited a relatively uniform distribution. The ZnO-doped Sb_2Te_3 composite films, especially with 5.2 at% ZnO concentration were found to have higher crystallization temperature, higher crystalline resistance, and faster crystallization speed in comparison with $Ge_2Sb_2Te_5$. A reversible repetitive optical switching behavior can be observed in $(ZnO)_{5.2}(Sb_2Te_3)_{94.8}$, confirming that the ZnO doping is responsible for a fast switching and the compound is stable with cycling. Therefore, it is promising for the applications in phase change memory devices.

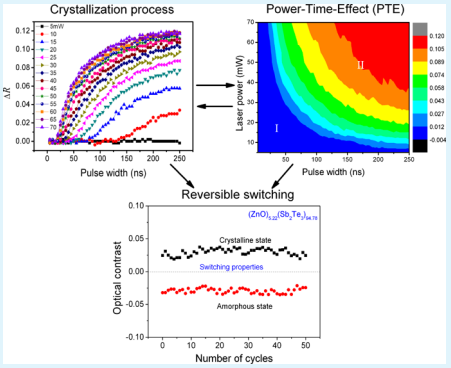

KEYWORDS: *thin films, nanocomposite, phase change, crystallization, optical reflectivity*

1. INTRODUCTION

Phase change memory (PCM) is an emerging nonvolatile random-access memory that exploits the unique behavior of chalcogenide alloys, e.g., these alloys can be repeatedly and rapidly switched between amorphous and crystalline phases with a drastic change in electrical resistances.[1,2] When the amorphous state with high resistance represents a binary "1", and the crystalline state with low resistance represents a "0",[3] the crystallization time scale is typically on the order of 100 ns.[4] Therefore, the alloys can be promising to be used as Flash memory with the potential to work at a speed currently reached by the volatile Dynamic Random Access Memory (DRAM).[5] Although the switching time and inherent scalability of PCM are promising, its temperature sensitivity is perhaps a bottleneck that may require changes in the production processing compatibly with the present technology.

Generally, a good phase change material should meet several requirements:[6] (1) the material should have an extremely short crystallization time in order to perform a fast switching speed in SET process; (2) the material should have a high crystallization temperature in order to increase 10-years data-retention ability; (3) the material is of a low melting temperature and high crystalline resistances so that it can reduce the RESET current in PCM; (4) the amorphous/crystalline resistance is large enough in order to obtain a large ON/OFF ratio; and (5) the material should have a smaller volume change due to crystallization, which can improve the SET/RESET programming cycles of PCM devices. Initial successful attempts at the PCM production were carried out using $Ge_2Sb_2Te_5$ (GST) material switching between a metastable rocksalt phase and the amorphous phase. The phase transition in the alloy is companied by a profound density change of 6.8%,[7] which has been suggested to be closely correlated with the large electrical contrast. The drawback of GST material as PCM devices are its high RESET current, relatively slow amorphous-to-crystalline speed, and poor thermal stability in the amorphous state. In contrast, other Sb−Te binary alloys that have been widely applied in phase change optical recording show higher crystallization speed than usual GST, and this is attributed to the growth-dominated crystallization mechanism. However, due to low crystallization temperature and poor data retention, Sb−Te binary alloys are not suitable for PCM application without further optimization. While a lot of attempts[8−11] have been applied to search various material alternatives to GST or Sb−Te, recently, the idea of using nanocomposite materials[12,13] have been developed in order to achieve high thermal stability and crystalline resistance while keeping fast crystallization speed. According to ref 14, defining smaller programming volume by formation of a composite film is an effective method to reduce power consumption. The composite film is

Received: March 6, 2014
Accepted: May 6, 2014
Published: May 6, 2014

characterized by several tens of nanometer scale clusters of phase change material, which is self-encapsulated by a dielectric material with high thermodynamical stability and low electrical conductivity, such as SiO_2, HfO_2, and TiO_2.[14−16] Therefore, nanocomposite materials are expected to possess appropriate thermal and electrical properties for PCM applications.

In this paper, we doped ZnO into Sb_2Te_3 in order to modify the properties of the materials for the potential applications in PCM. ZnO is a direct band gap (3.37 eV) semiconductor with excellent physical and chemical properties and thermodynamical stability at room temperature.[17] We further investigated the electrical resistances, thermal stability, and optical reflectivity of ZnO-doped Sb_2Te_3 and evaluated the microstructure and phase change mechanisms of the materials. Our aim was to screen the best material which meets all the requirements mentioned above for the applications in PCM.

2. EXPERIMENTAL SECTION

ZnO-doped Sb_2Te_3 nanocomposite films with a thickness of ∼200 nm were deposited on quartz and SiO_2/Si (100) substrates by a magnetron cosputtering method using individual ZnO and Sb_2Te_3 targets. In each run of the experiment, the chamber was evacuated to 1.4×10^{-4} Pa, and then Ar gas was introduced to 0.3 Pa for the film deposition. Pure Sb_2Te_3 and GST films with the same thickness were also prepared for comparison. The chemical composition of ZnO-doped Sb_2Te_3 films was measured using energy dispersive spectroscopy (EDS). The sheet resistances of as-deposited films as functions of elevated temperature (nonisothermal) and time at specific temperatures (isothermal) were *in situ* measured using a four-point probe in a homemade vacuum chamber. X-ray diffraction (XRD) was employed to characterize the structure of as-deposited and annealed ZnO-doped Sb_2Te_3 thin films. The diffraction patterns were taken in the 2θ range of 10-60° using Cu Kα radiation with a wavelength of 0.154 nm. Raman scattering spectra excited by 785 nm laser were recorded at room temperature using a backscattering configuration. During Raman spectra measurements, the power density on the sample was kept at low levels (∼0.2 mWμm^{-2}) in order to avoid any structural deformation induced by laser radiation. X-ray photoelectron spectroscopy (XPS) was used to examine the chemical bonding states of the elements. The microstructure of the composite film was analyzed by transmission electron microscopy (TEM). The 40 nm thick sample for TEM analysis was deposited on copper mesh with carbon film. The surface morphology was determined by atomic force microscopy (AFM). The optical transmission spectra of the films were measured using a UV-VIS-NIR spectrophotometer. A static laser tester (PST-1, NANOSstorage Co. Ltd., KOREA) with a wavelength of 658 nm was used to characterize crystallization behavior and optical switching test. The change of the laser power was from 5 mW to 70 mW, and that of the laser pulse width was from 5 to 250 ns.

3. RESULTS AND DISCUSSION

The sheet resistance (R_s) changes of GST, Sb_2Te_3, and ZnO-doped Sb_2Te_3 films with different annealing temperatures were presented in Figure 1. It can be seen that, Sb_2Te_3 film does not have an obvious abrupt drop of resistance because of a partial crystallization in the as-deposited state. In contrast, the GST film has transition of the resistance at 168 °C and 300 °C, respectively. Previously these two transitions have been assigned to amorphous to cubic and cubic to hexagonal transition, respectively.[18] For ZnO-doped Sb_2Te_3 films, a sudden drop of R_s occurs when the temperature reaches their individual crystallization temperature (T_c) of ZnO-doped Sb_2Te_3 films. The T_c, defined by the temperature corresponding to the minimum of the first derivation of the R-T curve, increases to ∼212, ∼217, ∼223, and ∼241 °C with increasing the Zn content of 0.6, 0.8, 1.7, and 5.2 at%, respectively. All the

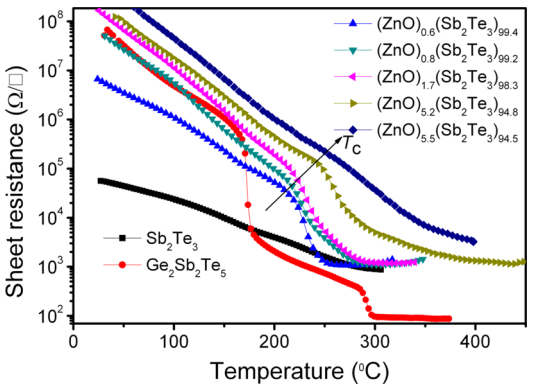

Figure 1. R-T curves of GST, Sb_2Te_3, and ZnO-doped Sb_2Te_3 films.

ZnO-doped Sb_2Te_3 films exhibit higher T_c than GST (∼168 °C) and Sb_2Te_3 (∼100 °C),[19] indicating that the addition of ZnO can improve the thermal stability of the Sb_2Te_3 films. However, when ZnO content is 5.5 at%, no significant abrupt change in sheet resistance can be observed, implying that excessive ZnO doping would retard the phase transition ability. This result shows that crystallization temperatures can be controlled by adjusting the ZnO content, and the optimal composition with good thermal stability can be confirmed to be $(ZnO)_{5.2}(Sb_2Te_3)_{94.8}$.

Compared with that in undoped Sb_2Te_3 films, the resistance ratio between the amorphous and crystalline states in $(ZnO)_{5.2}(Sb_2Te_3)_{94.8}$ film increases four to five orders of magnitude. The large resistance ratio can increase ON/OFF ratio values in PCM operation.[20] On the other hand, $(ZnO)_{5.2}(Sb_2Te_3)_{94.8}$ has higher resistance for both amorphous and crystalline states in comparison with Sb_2Te_3 and GST films, which is helpful to reduce the driving current for both set and reset operations of PCM.[21]

It is well known that thin films formed in vacuum usually exhibit more wrong-bonds compared with their bulk counterparts, and these wrong bonds (or heteropolar bonds) can form the localized states in amorphous solids and thus modify the optical band gap of the materials.[22] In order to understand the effect of doping on the optical band gap of the films, the optical transmittance (T_{op}) of the films were measured, and the absorption coefficient (α) can be calculated by using well known relation[23]

$$\alpha = (1/d)\ln(1/T_{op}) \quad (1)$$

where d is the thickness of the film.

Then, the optical band gap (E_{opt}) was also evaluated using the absorption properties, which were expressed as[23]

$$\alpha \cdot h\nu = B(h\nu - E_{opt})^2 \quad (2)$$

where $h\nu$ is the photon energy, and B is a parameter that depends on the electronic transition probability. $(\alpha \cdot h\nu)^{1/2}$ as a function of $h\nu$ (being photon energy in an unit of eV) was plotted in the main panel of Figure 2.

By extrapolating the linear portion of the curves to zero absorption, E_{opt} of the optimal $(ZnO)_{5.2}(Sb_2Te_3)_{94.8}$ film was determined to be 0.664 eV, which is higher than that of Sb_2Te_3 (0.307 eV). The results are in good agreement with the well-documented conclusion that amorphous GST usually exhibits a larger band gap than its crystalline counterpart.[22] The $(ZnO)_{5.2}(Sb_2Te_3)_{94.8}$ film is totally amorphous, while the

dx.doi.org/10.1021/am501345x | ACS Appl. Mater. Interfaces 2014, 6, 8488−8496

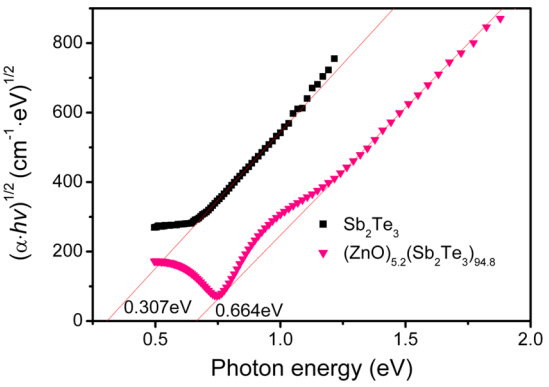

Figure 2. Tauc's plot of Sb_2Te_3 and $(ZnO)_{5.2}(Sb_2Te_3)_{94.8}$ films.

Sb_2Te_3 film contains crystalline grains as evident by XRD and Raman measurements below.

The XRD diffraction patterns of Sb_2Te_3 and ZnO-doped Sb_2Te_3 films with various annealing temperatures are presented in Figure 3.

As shown in Figure 3(a), with as-deposited Sb_2Te_3 film exhibits a broad band overlapping with one crystalline characteristic peak corresponding to Te (110), confirming that the nominal Sb_2Te_3 film actually contains some crystalline Te grains. At the annealing temperatures of 200 °C, a new Sb_2Te_3 phase that can be indexed with a R3m rhombohedral structure according to the PDF card of JCPDS NO.15-0874 forms, and XRD intensity corresponding to this phase becomes stronger with increasing annealing temperature. Moreover, a crystalline peak at $2\theta = 35.3°$ that can be assigned to the Sb_2O_3 phase appears at high annealing temperature of 300 °C and 350 °C due to the poor thermal stability of the Sb_2Te_3 film.

As for ZnO-doped Sb_2Te_3 films as shown in Figures 3(b)-3(f), all the as-deposited and 150 °C-annealed films exhibit an amorphous state. The crystalline peaks of Sb_2Te_3 appear in $(ZnO)_{0.6}(Sb_2Te_3)_{99.4}$ and $(ZnO)_{0.8}(Sb_2Te_3)_{99.2}$ films annealed at 200 °C, and the crystalline Sb_2O_3 peak appears at 250 °C as shown in Figures 3(b)-3(c). The intensity of all the peaks increases with increasing annealing temperature. In contrast, in the $(ZnO)_{1.7}(Sb_2Te_3)_{98.3}$ film as shown in Figure 3(d), the amorphous state is still kept at 200 °C. The crystalline peaks

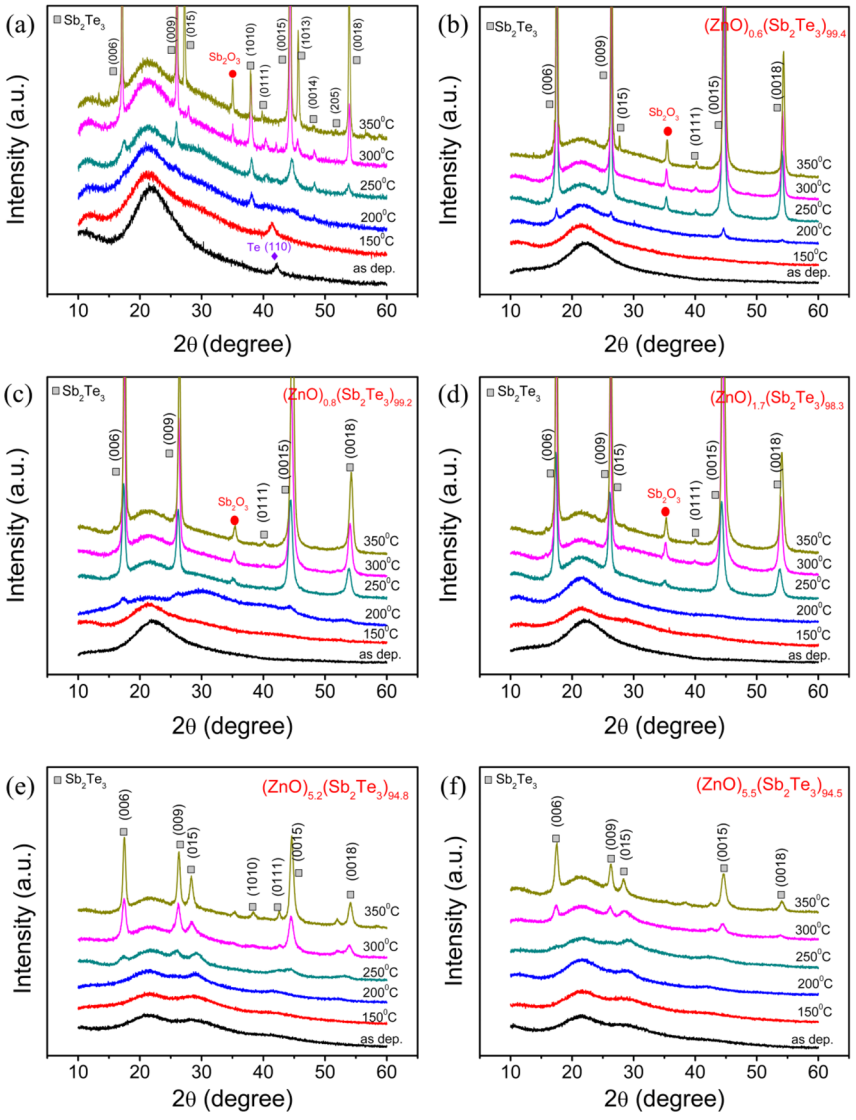

Figure 3. XRD patterns of as-deposited and annealed ZnO-Sb_2Te_3 films: (a) Sb_2Te_3, (b) $(ZnO)_{0.6}(Sb_2Te_3)_{99.4}$, (c) $(ZnO)_{0.8}(Sb_2Te_3)_{99.2}$, (d) $(ZnO)_{1.7}(Sb_2Te_3)_{98.3}$, (e) $(ZnO)_{5.2}(Sb_2Te_3)_{94.8}$, and (f) $(ZnO)_{5.5}(Sb_2Te_3)_{94.5}$.

dx.doi.org/10.1021/am501345x | ACS Appl. Mater. Interfaces 2014, 6, 8488−8496

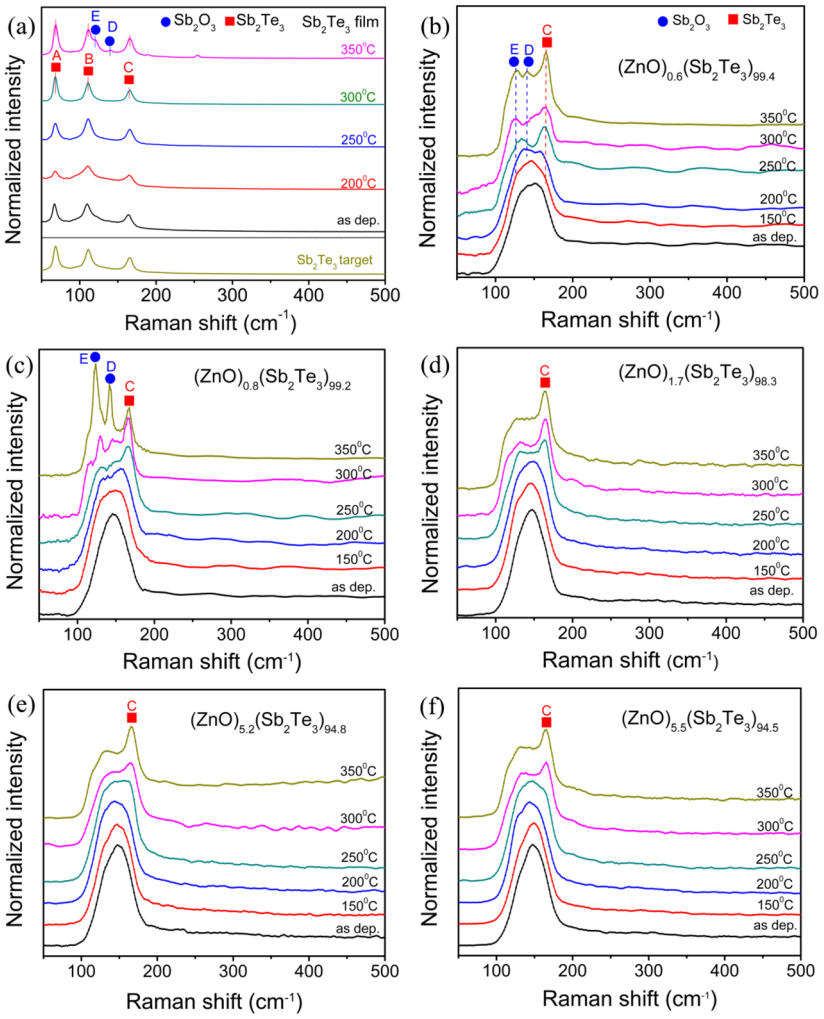

Figure 4. Raman spectra of as-deposited and annealed ZnO-Sb_2Te_3 films: (a) Sb_2Te_3, (b) $(ZnO)_{0.6}(Sb_2Te_3)_{99.4}$, (c) $(ZnO)_{0.8}(Sb_2Te_3)_{99.2}$, (d) $(ZnO)_{1.7}(Sb_2Te_3)_{98.3}$, (e) $(ZnO)_{5.2}(Sb_2Te_3)_{94.8}$, and (f) $(ZnO)_{5.5}(Sb_2Te_3)_{94.5}$.

that correspond to the rhombohedral Sb_2Te_3 phase appear at an annealing temperature of 250 °C, implying that the crystallization temperature increases. Nevertheless, the Sb_2O_3 phase still can be found in the $(ZnO)_{1.7}(Sb_2Te_3)_{98.3}$ film. With further increase of the ZnO doping content, $(ZnO)_{5.2}(Sb_2Te_3)_{94.8}$ and $(ZnO)_{5.5}(Sb_2Te_3)_{94.5}$ films as shown in Figures 3(e)-3(f) exhibit a single phase of rhombohedral Sb_2Te_3, and the Sb_2O_3 phase is totally suppressed in the $(ZnO)_{5.2}(Sb_2Te_3)_{94.8}$ and $(ZnO)_{5.5}(Sb_2Te_3)_{94.5}$ films due to the improvement in thermal stability, even at the annealing temperature of 350 °C. The Sb_2Te_3 crystalline peaks in Figures 3(e)-3(f) appear to be broader in width and lower in intensity with increasing ZnO doping. All these results indicate that, increasing the ZnO doping content could increase T_c, suppress the formation of Sb_2O_3, and restrain the growth of the crystalline grains.

Figures 4(a)-4(f) show Raman spectra of Sb_2Te_3 and ZnO-doped Sb_2Te_3 films. The target and the as-deposited film present the characteristics of stoichiometric Sb_2Te_3 at ~65 (peak A), ~110 (peak B), and ~165 cm^{-1} (peak C) as shown in Figure 4(a).[19,24,25] With increasing annealing temperature from 200 to 300 °C, Raman spectra exhibit negligible difference compared with those of the target and as-grown film, suggesting that they have quite similar microstructures. However, with further increasing annealing temperature to 350 °C, two new bands at ~123 cm^{-1} (peak E) and ~140 cm^{-1} (peak D) appear, which are ascribed to the vibrations of the Sb_2O_3 phases.[26]

We use these five peaks (A-D) as criterion to see how the ZnO doping can suppress the formation of crystalline Sb_2Te_3 and Sb_2O_3 phases. Figures 4(b)-4(c) are Raman spectra of the as-deposited and annealed $(ZnO)_{0.6}(Sb_2Te_3)_{99.4}$ and $(ZnO)_{0.8}(Sb_2Te_3)_{99.2}$ films, respectively. Raman spectra of the as-deposited and 150 °C-annealed $(ZnO)_{0.6}(Sb_2Te_3)_{99.4}$ films show a broad band in the range from 100 to 180 cm^{-1} as shown in Figure 4(b). The disappearance of the sharp peaks in Figure 4(a) demonstrate that a small amount of ZnO doping can effectively suppress the formation of the crystalline Sb_2Te_3 phase. The broad band evolutes into a band with two distinguishable peaks features in Raman spectrum of the film annealed at 250 °C and finally develops into three peaks with increasing annealing temperatures to 350 °C. As marked in Figure 4(b), the sharp peaks have the same positions as the peaks E, D, and C in Figure 4(a). Since the peaks E and D correspond to the vibrations of Sb_2O_3 and the peak C to that of crystalline Sb_2Te_3, the present results indicate that both crystalline Sb_2Te_3 and Sb_2O_3 phases can be formed in $(ZnO)_{0.6}(Sb_2Te_3)_{99.4}$ films annealed at higher temperature. The same conclusion can be drawn for the Raman spectra of $(ZnO)_{0.8}(Sb_2Te_3)_{99.2}$ films in Figure 4(c), which however exhibits much stronger peaks E and D at 300 °C.

dx.doi.org/10.1021/am501345x | ACS Appl. Mater. Interfaces 2014, 6, 8488−8496

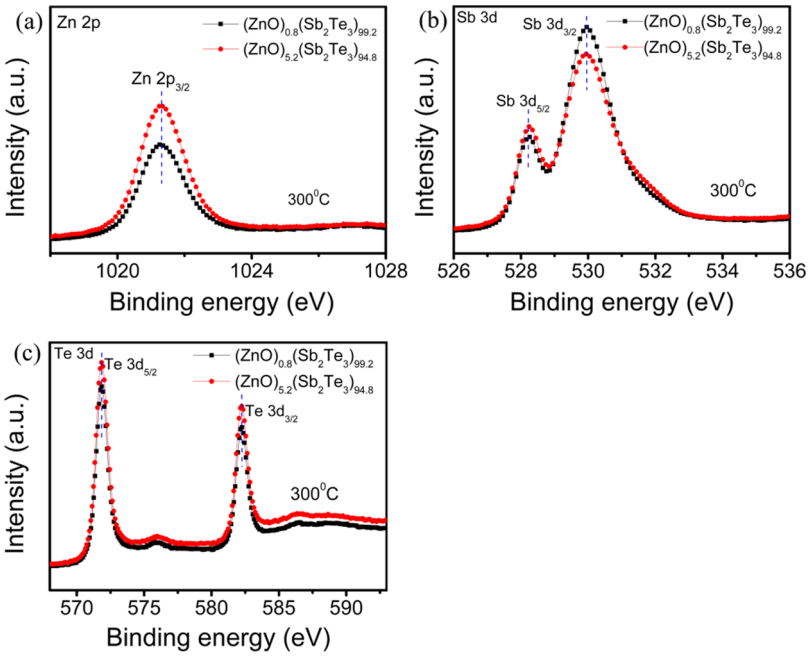

Figure 5. XPS spectra of ZnO-Sb_2 Te_3 phase-change films: (a) Zn 2p, (b) Sb 3d, and (c) Te 3d.

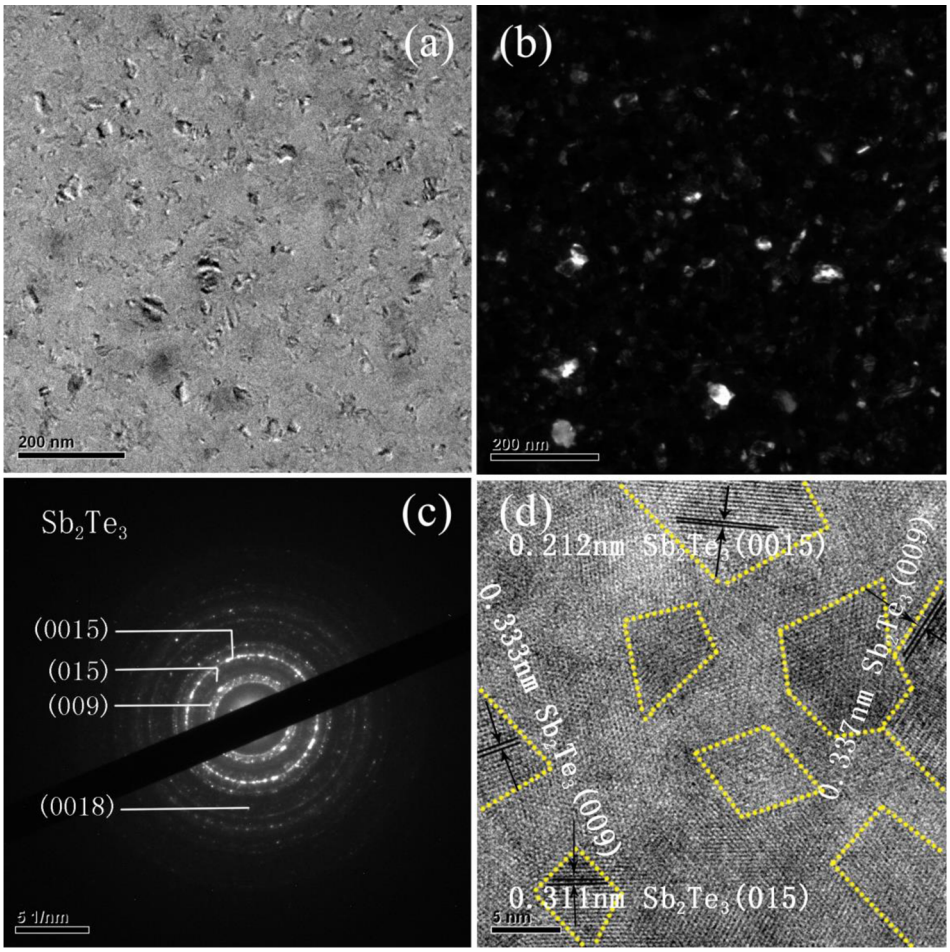

Figure 6. (a) The TEM BF micrograph, (b) the TEM DF micrograph, and (c) the SAED pattern of the $(ZnO)_{5.2}(Sb_2Te_3)_{94.8}$ film annealed at 300 °C. (d) The HRTEM images of the same film.

Let us go to Figures 4(d)-4(f) that correspond to the Raman spectra of $(ZnO)_{1.7}(Sb_2Te_3)_{98.3}$, $(ZnO)_{5.2}(Sb_2Te_3)_{94.8}$, and $(ZnO)_{5.5}(Sb_2Te_3)_{94.5}$ films. A common feature of Figures 4(d)-4(f) is that, with an increasing annealing temperature, a

dx.doi.org/10.1021/am501345x | ACS Appl. Mater. Interfaces 2014, 6, 8488−8496

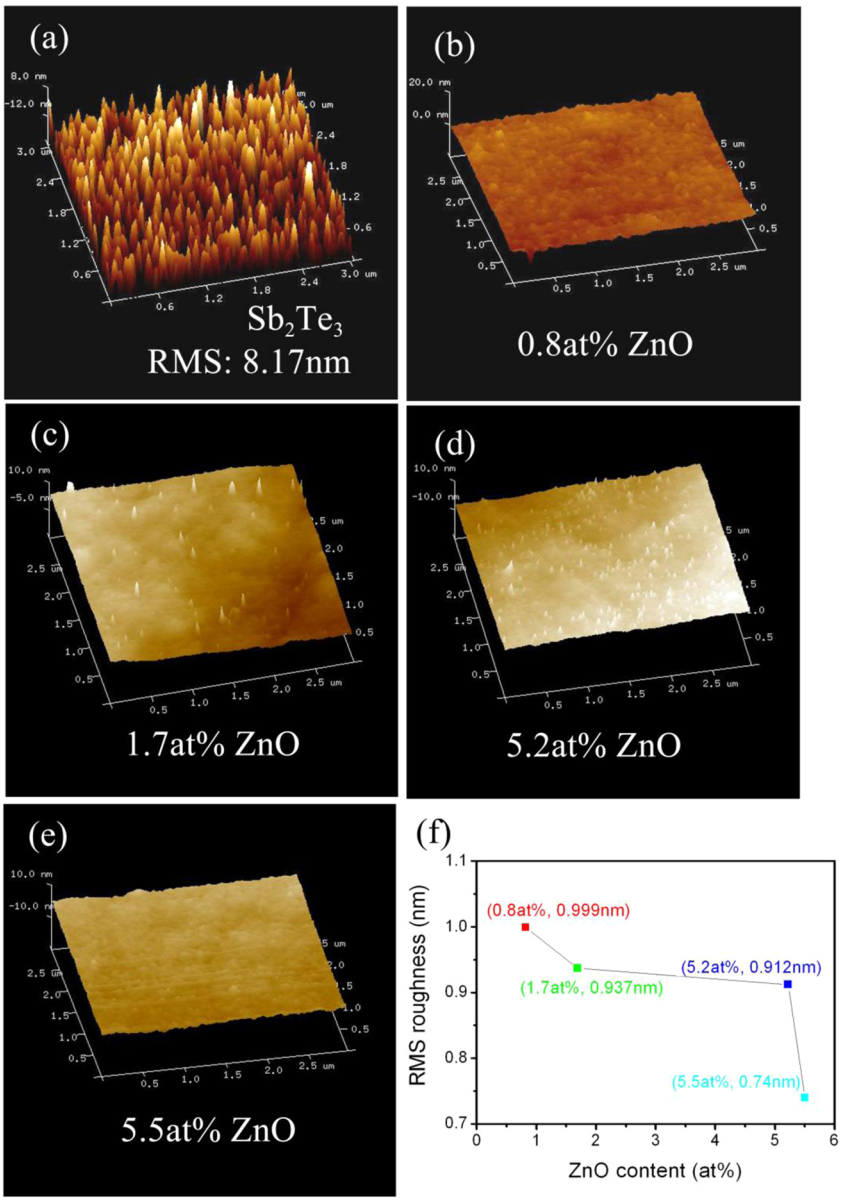

Figure 7. AFM images of nanocomposite ZnO-Sb_2Te_3 annealed at 300 °C for 3 min with different ZnO content: (a) 0, (b) 0.8 at%, (c) 1.7 at%, (d) 5.2 at%, and (e) 5.5 at%. (f) The relation between RMS and ZnO content.

sharp peak corresponding to peak C appears overlapping with the broad band from 100 to 180 cm^{-1}, and there is no any peak at the positions corresponding to peaks E and D. This is a symbol that the formation of oxidized Sb_2O_3 crystalline grains is totally suppressed with increasing content of ZnO doping.

The observations are in agreement with the XRD analysis, indicating that high ZnO-doping concentration can suppress the formation of the Sb_2O_3 phase and improve the thermal stability of $(ZnO)_x(Sb_2Te_3)_{1-x}$ films.

In order to examine whether Sb_2O_3 comes from surface oxidation, we employed XPS to measure the bonding structure of ZnO-Sb_2Te_3 films. Before doing that, the films were presputtered by Ar ions for 2 min to remove the possible surface oxidation layer of Sb_2O_3 formed during the annealing treatment or exposure in air.

Figures 5(a)-5(c) show the XPS Zn 2p, Sb 3d, and Te 3d spectra, respectively. It is obvious that the peak positions of Zn 2p almost keep no change with increasing ZnO content as shown in Figure 5(a), indicating that Zn atoms do not bond with Sb and Te atoms. This can be confirmed further in Figures 5(b)-5(c). The peak positions of Sb 3d and Te 3d exhibit no shift in binding energy in ZnO-doped Sb_2Te_3 films. This indicates that the Sb and Te atoms in Sb−Te bonds are not replaced by Zn or O atoms. We did not observe any new peaks that could be ascribed to Sb_2O_3 in Figure 5(b), indicating that Sb_2O_3 can be only formed in the surface of the film, and they have been removed by Ar ion sputtering. Previously, we have revealed that the introduction of Zn atoms in Zn−Sb−Te systems[27] could form Zn−Sb and Zn−Te bonds at the grain-boundaries. According to the results presented here, in the case of ZnO−Sb_2Te_3, no additional Zn−Sb and Zn−Te bonds can be formed. Combining with XRD and Raman scattering spectra where no peaks corresponding to the crystalline ZnO can be observed, we conclude that only amorphous ZnO exists in ZnO-Sb_2Te_3 films. In fact, ZnO has a high melting temperature (1975 °C)[17,28] and thus is relatively stable when ZnO−doped

dx.doi.org/10.1021/am501345x | ACS Appl. Mater. Interfaces 2014, 6, 8488−8496

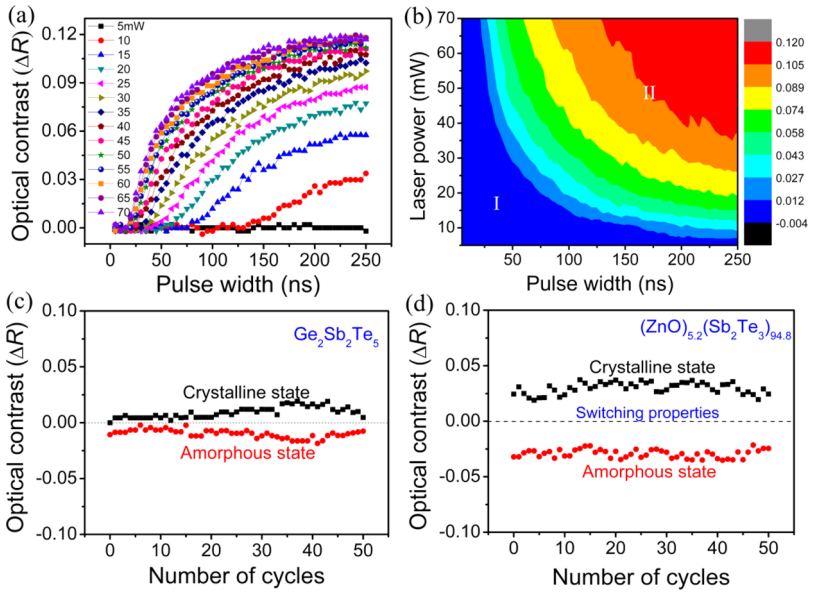

Figure 8. (a) Reflectivity changes of $(ZnO)_{5.2}(Sb_2Te_3)_{94.8}$ film with different laser power and pulse width; (b) PTE (power-time-effect) diagram of $(ZnO)_{5.2}(Sb_2Te_3)_{94.8}$ film. The optical switching behaviors during 50 cycles of operation on (c) the GST film and (d) the $(ZnO)_{5.2}(Sb_2Te_3)_{94.8}$ film.

Sb_2Te_3 films are annealed at 300 °C. On the other hand, the bond energy of Zn−O is larger than Sb−O and Te−O bonds. The thermodynamic stability of the oxides follows the order $ZnO > Sb_2O_3 > TeO_2$. Therefore, Zn has a priority to react with oxygen when the film was created in vacuum where the oxygen is deficient.

In order to investigate the distribution of crystalline grains in the ZnO-doped Sb_2Te_3 film, we measured bright-field (BF), dark-field (DF) TEM images, selected area electron diffraction (SAED) patterns, and high-resolution transmission electron microscopy (HRTEM) images of the optimal $(ZnO)_{5.2}(Sb_2Te_3)_{94.8}$ film. Figure 6(a) shows the BF TEM image of the $(ZnO)_{5.2}(Sb_2Te_3)_{94.8}$ film after 3 min heating at 300 °C. The crystallized film with a grain distribution in the range of 10−20 nm is in well agreement with the results estimated from the line width of XRD patterns. The DF TEM image in Figure 6(b) shows us the nanocrystals (white spots). The analysis of EDS (not shown here) indicates that the black (or dark) and white (or bright) domains in Figure 6(b) correspond to ZnO-rich and Sb_2Te_3-rich phases, respectively. Again, this demonstrates the amorphous nature of ZnO in the $(ZnO)_{5.2}(Sb_2Te_3)_{94.8}$ film. This result is very important for development of PCM. On one hand, current can be confined in the Sb_2Te_3 domains. On the other hand, the segregated domains exhibit relatively uniform distribution, and thus the ZnO-Sb_2Te_3 phase change layer would have a small programming volume and may exhibit significantly reduced operating power, with relatively small cell-to-cell variation.[14,29]

Noteworthy is that the SAED pattern of the $(ZnO)_{5.2}(Sb_2Te_3)_{94.8}$ film in Figure 6(c) suggests a phase of Sb_2Te_3, which is in agreement with the XRD analysis. HRTEM images as shown in Figure 6(d) make it possible to measure the interplanar distances, which are in agreement with those of crystalline Sb_2Te_3. No other crystalline phase was observed in the film. Based on all the analysis above, a nanocomposite structure with mixed amorphous ZnO and crystalline Sb_2Te_3 phases is confirmed.

Film surface roughness is extremely important for device performance, since electrical properties depend on not only a well-defined microstructure but also the quality of the electrode-film interface. Figures 7(a)-7(e) show the AFM images of Sb_2Te_3 and ZnO-doped Sb_2Te_3 films annealed at 300 °C. Figure 7(f) is the root mean square (RMS) roughness of the films as a function of ZnO-doping concentration. The scan area in Figures 7(a)-7(e) is 1 μm × 1 μm. RMS roughness of the Sb_2Te_3 thin films is 8.17 nm as shown in Figure 7(a), and this is attributed to its larger grain size. The decrease of the RMS roughness with increasing ZnO concentration as shown in Figure 7(f) can be attributed to the smaller grain size, indicating that increasing the ZnO concentration can improve the surface quality of the films. So we can infer that the $(ZnO)_{5.2}(Sb_2Te_3)_{94.8}$ phase change films have a smoother and uniform surface.

Phase change speed is one of the most important parameters of phase-change materials as it affects the data switching rate for a PCM.[30] In order to characterize phase change behavior and crystallization time of the $(ZnO)_{5.2}(Sb_2Te_3)_{94.8}$ film, a static tester using pulsed laser irradiation was employed, where the power was increased up to 70 mW, and the width of the laser pulses was increased from 5 to 250 ns. The optical contrast (ΔR) of a phase change material is one of the most important optical parameters in phase change storage.[31] It can be defined by the following equation: $\Delta R = (R_{after} - R_{before})/R_{before}$, where R_{before} and R_{after} indicate the reflectivity before and after irradiation, respectively. Figures 8(a) and 8(b) show the optical contrast as a function of pulse width and power-time-effect (PTE) diagrams for the $(ZnO)_{5.2}(Sb_2Te_3)_{94.8}$ film, respectively. The significant increases of ΔR values are found almost in the whole crystallization process with the laser power and pulse width increasing. The magnitude of ΔR can be further illustrated using the different colors in the PTE diagram. With a lower laser power of 5 mW, reflectivity does not change with pulse width increasing (region I), because the applied laser power was insufficient to initiate crystallization. As the laser power is increased, the film receives sufficient energy gradually to overcome the activation barrier. Thus, crystallization occurs and ΔR increases (region II).[32,33] When the laser powers were 10, 30, 50, and 70 mW, the minimum times for crystallization

of GST were 300, 150, 80, and 40 ns, respectively, reported in our previous work.[34] In case of the $(ZnO)_{5.2}(Sb_2Te_3)_{94.8}$ film, its minimum times for crystallization were 130, 40, 20, and 10 ns, respectively, when the same power is applied in the sample, illustrating that the crystallization speed of the film is faster than GST.

To confirm the stability of the structure during repetitive melt-quenching cycles, we checked the optical switching behavior of the GST and $(ZnO)_{5.2}(Sb_2Te_3)_{94.8}$ films. The laser power and pulse width for crystallization and melting of GST and $(ZnO)_{5.2}(Sb_2Te_3)_{94.8}$ films was 35 mW−250 ns and 70 mW−100 ns. Figures 8(c) and 8(d) show reliable optical switching behaviors in the GST and $(ZnO)_{5.2}(Sb_2Te_3)_{94.8}$ films during 50 cycles of operation. We can see that the differences in ΔR between crystallization and amorphization recording were sustained by relatively constant values, which indirectly supports the fact that the nanocomposite structure of $(ZnO)_{5.2}(Sb_2Te_3)_{94.8}$ is sustained and the compound is stable under repetitive melt-quenching and crystallization-switching cycles.

4. CONCLUSIONS

We investigated ZnO-doped Sb_2Te_3 films in order to achieve superior phase change materials with better thermal stability and electrical properties while maintaining other advantages of Sb_2Te_3 materials. The addition of ZnO could increase crystallization temperature and crystalline resistance, suppress the formation of Sb_2O_3, and restrain the growth of the Sb_2Te_3 crystalline grains. Sb_2Te_3-rich nanocrystals are surrounded by the ZnO-rich amorphous phase in the $(ZnO)_{5.2}(Sb_2Te_3)_{94.8}$ film, and the segregated domains exhibit relatively uniform distribution. The $(ZnO)_{5.2}(Sb_2Te_3)_{94.8}$ film exhibits a smooth and uniform surface. The minimum times for crystallization of the $(ZnO)_{5.2}(Sb_2Te_3)_{94.8}$ film is revealed to be as short as ∼10 ns at a given proper laser power of 70 mW. The reliable repetitive switching behavior of the film can be also verified in the $(ZnO)_{5.2}(Sb_2Te_3)_{94.8}$ film, confirming that the film composition is stable with cycling. All these suggest a huge potential of $(ZnO)_{5.2}(Sb_2Te_3)_{94.8}$ used in PCM.

AUTHOR INFORMATION

Corresponding Authors

*Phone: +86-574 87600947. Fax: +86-574 87600946. E-mail: guoxiang_568@163.com (G.W.).
*E-mail: shenxiang@nbu.edu.cn (X.S.).
*E-mail: nieqiuhua@nbu.edu.cn (Q.N.).

Notes

The authors declare no competing financial interest.

ACKNOWLEDGMENTS

This work was financially supported by the International Science & Technology Cooperation Program of China (Grant No. 2011DFA12040), the National Program on Key Basic Research Project (973 Program) (Grant No. 2012CB722703), the Natural Science Foundation of China (Grant Nos. 61306147 and 61377061), the Program for Innovative Research Team of Ningbo city (Grant No. 2009B21007), and the Young Leaders of the academic climbing project of the Education Department of Zhejiang Province (Grant No. pd2013092) and sponsored by the K. C. Wong Magna Fund at Ningbo University.

REFERENCES

(1) Loke, D.; Lee, T. H.; Wang, W. J.; Shi, L. P.; Zhao, R.; Yeo, Y. C.; Chong, T. C.; Elliott, S. R. Breaking the Speed Limits of Phase-Change Memory. *Science* **2012**, *336*, 1566−1569.
(2) Atwood, G. Engineering: Phase-Change Materials for Electronic Memories. *Science* **2008**, *321*, 210−211.
(3) Song, K. H.; Kim, S. W.; Seo, J. H.; Lee, H. Y. Influence of the Additive Ag for Crystallization of Amorphous Ge-Sb-Te Thin Films. *Thin Solid Films* **2009**, *517*, 3958−3962.
(4) Wuttig, M.; Steimer, C. Phase Change Materials: From Material Science to Novel Storage Devices. *Appl. Phys. A: Mater. Sci. Process.* **2007**, *87*, 411−417.
(5) Lencer, D.; Salinga, M.; Wuttig, M. Design Rules for Phase-Change Materials in Data Storage Applications. *Adv. Mater.* **2011**, *23*, 2030−2058.
(6) Wuttig, M.; Yamada, N. Phase-Change Materials for Rewriteable Data Storage. *Nat. Mater.* **2007**, *6*, 824−832.
(7) Welnic, W.; Wuttig, M. Reversible Switching in Phase-Change Materials. *Mater. Today* **2008**, *11*, 20−27.
(8) Zhou, X. L.; Wu, L. C.; Song, Z. T.; Rao, F.; Ren, K. Phase Transition Characteristics of Al-Sb Phase Change Materials for Phase Change Memory Application. *Appl. Phys. Lett.* **2013**, *103*, 072114 [5 pages].
(9) Rao, F.; Song, Z. T.; Ren, K.; Zhou, X. L.; Cheng, Y.; Wu, L. C.; Liu, B. Si−Sb−Te Materials for Phase Change Memory Applications. *Nanotechnology* **2011**, *22*, 145702−145711.
(10) Kao, K. F.; Lee, C. M.; Chen, M. J.; Tsai, M. J.; Chin, T. S. $Ga_2Te_3Sb_5$-A Candidate for Fast and Ultralong Retention Phase-Change Memory. *Adv. Mater.* **2009**, *21*, 1695−1699.
(11) Borisenko, K. B.; Chen, Y. X.; Cockayne, D. J. H.; Song, S. A.; Jeong, H. S. Understanding Atomic Structures of Amorphous C-Doped $Ge_2Sb_2Te_5$ Phase-Change Memory Materials. *Acta Mater.* **2011**, *59*, 4335−4342.
(12) Wang, C. Z.; Li, S. M.; Zhai, J. W.; Shen, B.; Sun, M. C.; Lai, T. S. Rapid Crystallization of $SiO_2/Sb_{80}Te_{20}$ Nanocomposite Multilayer Films for Phase-Change Memory Applications. *Scripta Mater.* **2011**, *64*, 645−648.
(13) Ryu, S. W.; Oh, J. H.; Cho, B. J.; Hwang, S. Y.; Hong, S. K.; Hwang, C. S.; Kim, H. J. SiO_2 Incorporation Effects in $Ge_2Sb_2Te_5$ Films Prepared by Magnetron Sputtering for Phase Change Random Access Memory Devices. *Electrochem. Solid-State Lett.* **2006**, *9*, G259−G261.
(14) Song, S. N.; Song, Z. T.; Liu, B.; Wu, L. C.; Feng, S. L. Performance Improvement of Phase-Change Memory Cell With $Ge_2Sb_2Te_5$-HfO_2 Composite Films. *Appl. Phys. A: Mater. Sci. Process.* **2010**, *99*, 767−770.
(15) Lee, T. Y.; Yim, S. S.; Lee, D.; Lee, M. H.; Ahn, D. H.; Kim, K. B. Separate Domain Formation in $Ge_2Sb_2Te_5$-SiO_x Mixed Layer. *Appl. Phys. Lett.* **2006**, *89*, 163503 [3 pages].
(16) Lee, D.; Yim, S. S.; Lyeo, H. K.; Kwon, M. H.; Kang, D.; Jun, H. G.; Nam, S. W.; Kim, K. B. Formation of $Ge_2Sb_2Te_5$-TiO_x Nanostructures for Phase Change Random Access Memory Applications. *Electrochem. Solid-State Lett.* **2010**, *13*, K8−K11.
(17) Pearton, S. J.; Norton, D. P.; Steiner, I. Recent Progress in Processing and Properties of ZnO. *Superlattices Microstruct.* **2003**, *34*, 3−32.
(18) Wang, G. X.; Nie, Q. H.; Shen, X.; Wang, R. P.; Wu, L. C.; Fu, J.; Xu, T. F.; Dai, S. X. Phase Change Behaviors of Zn-Doped $Ge_2Sb_2Te_5$ Films. *Appl. Phys. Lett.* **2012**, *101*, 051906 [5 pages].
(19) Sosso, G. C.; Caravati, S.; Bernasconi, M. Vibrational Properties of Crystalline Sb_2Te_3 From First Principles. *J. Phys.: Condens. Matter* **2009**, *21*, 095410 [6 pages].
(20) Kang, M. J.; Choi, S. Y.; Wamwangi, D.; Wang, K.; Steimer, C.; Wuttig, M. Structural Transformation of Sb_xSe_{100-x} Thin Films for Phase Change Nonvolatile Memory Applications. *J. Appl. Phys.* **2005**, *98*, 014904 [6 pages].
(21) Zhou, X. L.; Wu, L. C.; Song, Z. T.; Cheng, Y.; Rao, F.; Ren, K.; Song, S. N.; Liu, B.; Feng, S. L. Nitrogen-Doped Sb-Rich Si-Sb-Te

Phase-Change Material for High-Performance Phase-Change Memory. *Acta Mater.* **2013**, *61*, 7324−7333.
(22) Pirovano, A.; Lacaita, A. L.; Benvenuti, A.; Pellizzer, F.; Bez, R. Electronic Switching in Phase-Change Memories. *IEEE Trans. Electron Devices* **2004**, *51*, 452−459.
(23) Tauc, J. *Amorphous and Liquid Semiconductors*; Plenum Press: New York, 1974; p 171.
(24) Shahil, K. M. F.; Hossain, M. Z.; Goyal, V.; Balandin, A. A. Micro-Raman Spectroscopy of Mechanically Exfoliated Few-Quintuple Layers of Bi_2Te_3, Bi_2Se_3, and Sb_2Te_3 Materials. *J. Appl. Phys.* **2012**, *111*, 054305 [8 pages].
(25) Wang, G. X.; Nie, Q. H.; Shen, X.; Wang, R. P.; Wu, L. C.; Lv, Y. G.; Fu, J.; Xu, T. F.; Dai, S. X. Advantages of $Zn_{1.25}Sb_2Te_3$ Material for Phase Change Memory. *Mater. Lett.* **2012**, *87*, 135−138.
(26) Jang, M. H.; Park, S. J.; Lim, D. H.; Cho, M. H.; Do, K. H.; Ko, D. H.; Sohn, H. C. Phase Change Behavior in Oxygen-Incorporated $Ge_2Sb_2Te_5$ Films. *Appl. Phys. Lett.* **2009**, *95*, 012102 [3 pages].
(27) Shen, X.; Wang, G. X.; Wang, R. P.; Dai, S. X.; Wu, L. C.; Chen, Y. M.; Xu, T. F.; Nie, Q. H. Enhanced Thermal Stability and Electrical Behavior of Zn-Doped Sb_2Te Films for Phase Change Memory Application. *Appl. Phys. Lett.* **2013**, *102*, 131902 [4 pages].
(28) Pearton, S. J.; Norton, D. P.; Ip, K.; Heo, Y. W.; Steiner, T. Recent Progress in Processing and Properties of ZnO. *Prog. Mater. Sci.* **2005**, *50*, 293−340.
(29) Lu, Y. G.; Song, S. N.; Song, Z. T.; Wu, L. C.; Liu, B.; Feng, S. L.; Guo, X. H. Study on TiO_2-Doped Ge_2Te_3 Films for Phase-Change Memory Application. *J. Phys. D: Appl. Phys.* **2011**, *44*, 145102−145108.
(30) Hu, Y. F.; Li, S. M.; Lai, T. S.; Song, S. N.; Song, Z. T.; Zhai, J. W. Fast Crystallization and Low Power of Al-Doped Sn_2Se_3 Thin Films for Phase Change Memory Applications. *J. Alloys Compd.* **2013**, *581*, 515−518.
(31) Detemple, R.; Wamwangi, D.; Bihlmayer, G.; Wuttig, M. Identification of Te Alloys with Suitable Phase Change Characteristics. *Appl. Phys. Lett.* **2003**, *83*, 2572 [3 pages].
(32) Park, S. J.; Jang, M. H.; Park, S. J.; Cho, M. H.; Ko, D. H. Characteristics of Phase Transition and Separation in a In−Ge−Sb−Te System. *Appl. Surf. Sci.* **2012**, *258*, 9786−9791.
(33) Park, T. J.; Choi, S. Y.; Kang, M. J. Phase Transition Characteristics of Bi/Sn Doped $Ge_2Sb_2Te_5$ Thin Film for PRAM Application. *Thin Solid Film* **2007**, *515*, 5049−5053.
(34) Wang, G. X.; Shen, X.; Nie, Q. H.; Wang, R. P.; Wu, L. C.; Lu, Y. G.; Dai, S. X.; Xu, T. F.; Chen, Y. M. Improved Phase-Change Characteristics of Zn-Doped Amorphous Sb_7Te_3 Films for High-Speed and Low-Power Phase Change Memory. *Appl. Phys. Lett.* **2013**, *103*, 031914 [5 pages].